Magnetic nanobelts of iron-doped zinc oxide

Yu, M. B.; Xiong, Y. Z.; Chen, J. S.; Xu, Chunxiang; Sun, Xiaowei; Dong, Zhili

2005

Xu, C., Sun, X., Dong, Z. L., Yu, M. B., Xiong, Y. Z. & Chen, J. S. (2005). Magnetic nanobelt of iron-doped zinc oxide. Applied Physics Letters, 86.

https://hdl.handle.net/10356/93936

https://doi.org/10.1063/1.1919391

Magnetic nanobelts of iron-doped zinc oxide

C. X. Xu[a] and X. W. Sun[b]
School of Electric and Electronic Engineering, Nanyang Technological University, Nanyang Avenue, Singapore 639798, Singapore

Z. L. Dong
School of Materials Science and Engineering, Nanyang Technological University, Nanyang Avenue, Singapore 639798, Singapore

M. B. Yu and Yong Zhong Xiong
Institute of Microelectronics, 11 Science Park Road, Science Park II, Singapore 117684, Singapore

J. S. Chen
Data Storage Institute, 5 Engineering Drive 1, Singapore 117684, Singapore

(Received 29 July 2004; accepted 9 March 2005; published online 21 April 2005)

Magnetic nanobelts of iron-doped zinc oxide were fabricated by vapor–phase transport using zinc oxide, iron oxide, and graphite as source materials. The nanobelts grew mainly along $[10\bar{1}0]$ orientation and enclosed by $\pm(0001)$ and $\pm(\bar{1}2\bar{1}0)$ surfaces. The measurements of x-ray diffraction, energy-dispersive x-ray spectroscopy, and high-resolution transmission electron microscopy demonstrated that iron was doped into the nanobelts. As a result, the nanobelts were magnetic.
 [DOI: 10.1063/1.1919391]

Nanostructrual zinc oxide (ZnO) has attracted much interest because of its unique optoelectric properties, aesthetic morphologies, and versatile applications. Recently, various ZnO nanostructures have been utilized to fabricate nanodevices, such as nanolaser,[1] field emission array,[2–4] field effect transistor,[5,6] photosensor,[5,6] gas sensor,[5] optical switch,[5] and piezoelectric device.[7] Meanwhile, the investigation on diluted magnetic semiconductors (DMS) demonstrated an application of ZnO as a host material for spintronic devices,[8–10] which make use of electron spin instead of charge for data reading and writing. To integrate the DMS into present electronics, low-dimensional structures are required for exploiting the advantages offered by the spin.[11] However, the research is mainly focused on bulk or thin film materials so far,[9,10] except for a few reports published recently on magnetic nanorods and nanobelts of ZnO fabricated by implanting transitional elements such as manganese and cobalt.[11,12] Comparing to the typical magnetic materials, the nanostructural DMS is expected to find applications in information storage with higher density, faster speed, and less power consumption. Moreover, the DMS can also be used for electronics, quantum computing, and optical encoder. In this letter, we shall report nanobelts of iron-doped ZnO fabricated by a vapor-phase transport (VPT) method and their magnetic properties. This quasi-one-dimensional structure is a potential candidate for spintronics.

The fabrication process of the VPT is similar to our previous reports.[3,4] In brief, the mixture of zinc oxide, iron oxide, and graphite powders was employed as source material. The source material of mixed powders was sintered at 1150 °C for 1 h in a tube furnace in air. The product was collected on a silicon wafer at about 850–950 °C. After fabrication, the as-deposited materials were examined by scanning electron microscopy (SEM), transmission electron microscopy (TEM) and x-ray diffraction (XRD) to characterize the morphology and crystal structure. Energy-dispersive x-ray spectroscope (EDX) attached to the TEM was employed to detect the chemical composition of the nanostructure. Magnetic properties of nanobelts were measured using vibrating sample magnetometer (VSM). All measurements were carried out at room temperature.

Figures 1(a) and 1(b) show the SEM images of as-deposited product with low and high magnification, respectively. The morphology shown in Fig. 1 clearly illustrates a nanobelt structure with smooth surfaces. The length of the nanobelts is in the order of several hundred microns, the width is about several hundred nanometers to 1.5 μm, and the thickness is about 50 nm. Figure 2 shows the XRD pattern of the nanobelts shown in Fig. 1. It can be seen that the dominant diffraction peaks, as indexed in the spectrum, are originated from wurtzite structural ZnO with the lattice constants of $a=0.325$ nm and $c=0.5207$ nm. Since it is a well-known morphology of ZnO, the nanobelt should be made up of ZnO primarily. It is also noted that some weak diffraction peaks appear on the XRD spectrum which are related to the incorporated iron. It is difficult to identify the exact origin of these week peaks because the XRD data of iron oxide (Fe_2O_3 and Fe_3O_4) and Zn–Fe–O complex ($ZnFe_2O_4$) are closed to the peak positions. It is noticeable that all of the weak peaks show shift relative to the standard data of the labeled compounds in Fig. 2. For example, the labeled peaks for Fe_2O_3 at 25.6°, 49.2°, 54.4°, and 64.8° are corresponding to the standard data of 24.2° (012), 49.5° (024), 54.2° (116), and 64.2° (214), respectively. The shift in peak position is significant. However, the largest shift for ZnO diffraction angles is 0.2° compared to the standard data, which can be considered as experimental error. The large shift of iron oxides/compounds and small shift of ZnO indicate the interaction between ZnO and iron, even the guest element exists as iron complex clusters in the host.

[a]Also with Department of Electronic Engineering, Southeast University, Nanjing 210096, P. R. China.
[b]Author to whom correspondence should be addressed; electronic mail: exwsun@ntu.edu.sg

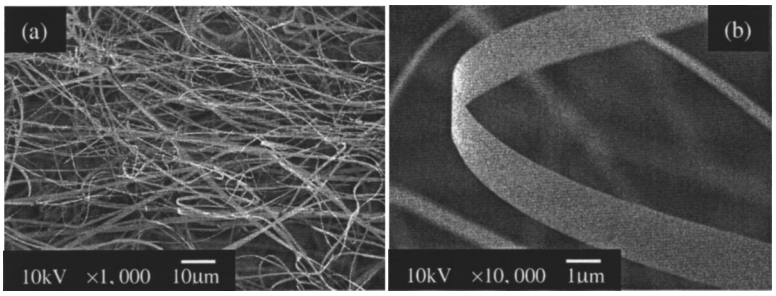

FIG. 1. SEM images of the ZnO nanobelts with low (a) and high (b) magnification.

Figure 3 shows TEM images of an individual ZnO nanobelt under low (a) and high (b) and (c) resolution, respectively. The lattice fringes are clearly seen in Fig. 3(b). The inset in Fig. 3(b) shows the selected area electron diffraction (SAED) pattern of the nanobelt from zone axis $[\bar{1}2\bar{1}0]$. The diffraction pattern (after converting the direction indices from reciprocal lattice to direct lattice) demonstrates that lattice orientation is along [0001] in the width direction and along $[10\bar{1}0]$ in the length direction. Consistent with the SAED pattern, the measured *d*-spacing along the width direction in Fig. 3(b) corresponds to the interplanar spacing 0.26 nm of (0002). From the SAED pattern, it can also be estimated according to vector algorithm that the up and bottom surfaces are $\pm(\bar{1}2\bar{1}0)$ planes.

In order to obtain magnetic nanostructures, ion implantation was previously employed to introduce Mn and Co into ZnO nanobelts and nanorods.[11,12] In the Mn-doped nanobelts, Ronning *et al.*[11] observed stacking fault through the back and front fast Fourier transformation analysis using the electron diffraction spots of ±(0002) planes. The dislocations were assumed being related to the dopants. In the present case, the desired dopant iron was added into the source materials and was observed in ZnO nanobelts through the XRD data. It is noticeable that some lattice distortions appear in Fig. 3(c). The white and black arrows mark the stacking faults and the bending of lattice fringes respectively in Fig. 3(c). These defects in lattice are direct indication of impurity (iron) incorporation.

The vapor–liquid–solid (VLS) mechanism[1,4] can be used to interpret the growth process of the nanobelts. The zinc vapor generated by carbon thermal reduction of ZnO condenses to liquid droplets and oxidizes into ZnO nucleus. In general, the ZnO nanostructure grows along [0001] orientation because of the lowest binding energy in this direction. In some conditions, such as high vapor pressure and high growth temperature, however, the surfaces with lower energy tend to grow larger and remain flat, and finally determine the enclosure of the surface. The incoming vapor is adsorbed at the front facet of the structure which grows up into a long belt. In present case, the nanobelts grow along $[10\bar{1}0]$ orientation and enclosed by ±(0001) and $\pm(\bar{1}2\bar{1}0)$ surfaces, as shown in Fig. 3(b). During the growth process, both zinc and

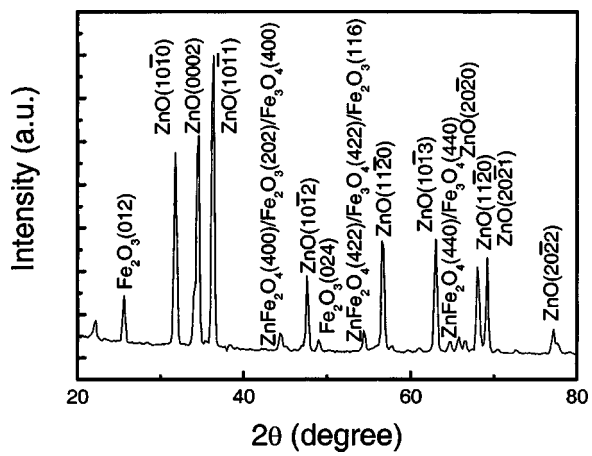

FIG. 2. XRD pattern of the iron-containing ZnO nanobelts. Crystallographic planes of ZnO and possible iron compounds are labeled.

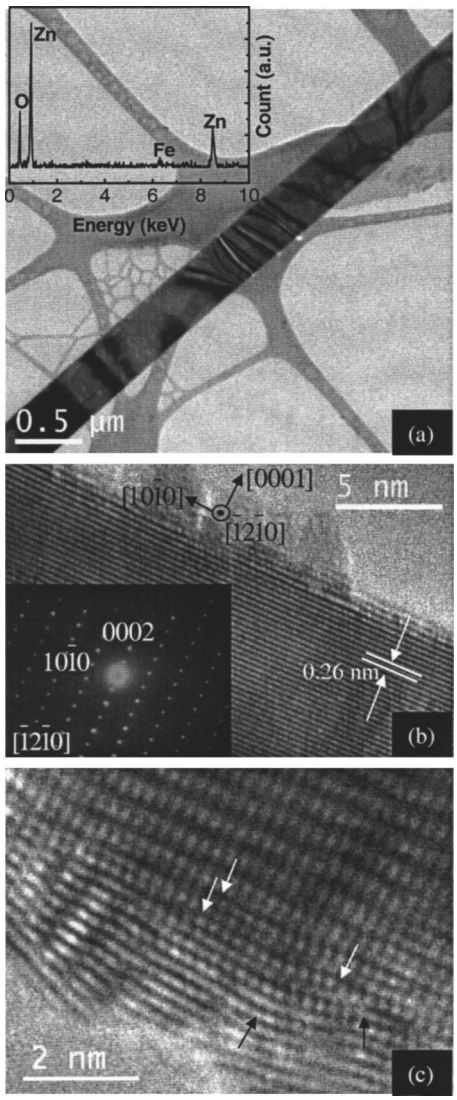

FIG. 3. (a) Low magnification TEM image of a nanobelt inserted with the EDX spectrum; (b) a high resolution TEM image of the nanobelt edge with SAED pattern inserted; and (c) a high resolution TEM image of a nanobelt edge. The white and black arrows in (c) mark the stacking faults and the bending of lattice fringes, respectively.

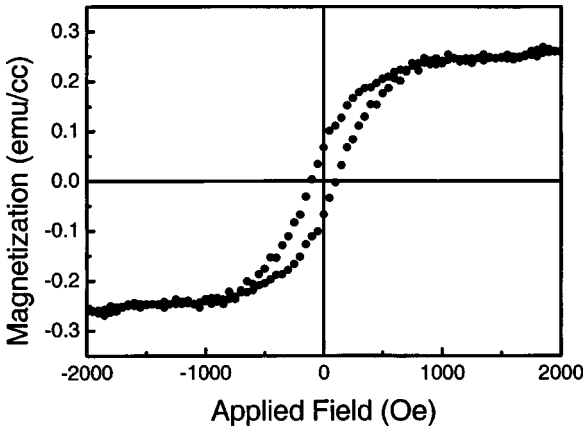

FIG. 4. Hysteresis loop of magnetization **M** vs applied magnetic field **H** detected at room temperature by VSM method.

iron can function as the catalysts. The iron catalyst should originate from the thermal carbon reduction of iron oxide. From our EDX measurement as shown in Fig. 3(a), the iron signal could be observed throughout the whole nanobelt. The chemical compositions are 44.45 at. % of O, 53.98 at. % of Zn, and 1.58 at. % of Fe, according to the EDX spectrometer's own computer program. It is worth mentioning that, the composition obtained here serves only as an evidence of the existence of Fe in the sample, as in general, there is about 1% error in the composition analysis from EDX. On the other hand, we could not observe any particle-like features existing at the ends of nanobelts examined. Thus, it is likely that iron was incorporated into the nanobelt while it catalyzed the nanobelt growth. The high-resolution TEM [Fig. 3(c)] further confirms that impurities were incorporated into the nanobelt causing stacking faults and lattice distortions.

Because of the existence of iron, the nanobelts were magnetized when a magnetic field is applied. Figure 4 shows the hysteresis loop of the magnetization **M** as a function of the applied magnetic field **H**. It can be seen that the saturation magnetization $\mathbf{M_s}$ is about 0.24 emu/cc corresponding to a saturation field of about 800 Oe. As shown in the inset of Fig. 4, the coercive field $\mathbf{H_c}$ is about 103 Oe and the remanent magnetization $\mathbf{M_r}$ is about 0.065 emu/cc. The calculated squareness of the hystersis loop is 0.27.

In conclusion, iron-doped ZnO nanobelts were fabricated based on a VLS process. The nanobelts grew along $[10\bar{1}0]$ orientation and enclosed by $\pm(0001)$ and $\pm(\bar{1}\bar{2}10)$ surfaces. During the growth process, iron generated from the carbon thermal reduction of iron oxide not only acted as a catalyst (together with zinc) but also diffused into the nanobelt. The ZnO nanobelts showed a hysteresis loop of **M**–**H** due to the doping of iron.

The authors gratefully acknowledge sponsorships from Research Grant Manpower Fund (RG51/01) of Nanyang Technological University and Science and Engineering Research Council Grant (No. 0421010010) from the Agency for Science, Technology and Research (A*STAR), Singapore.

[1] M. Huang, S. Mao, H. Feick, H. Yan, Y. Wu, H. Kind, E. Weber, R. Russo, and P. Yang, Science **292**, 1897 (2001).
[2] C. J. Lee, T. J. Lee, S. C. Lyu, Y. Zhang, H. Ruh, and H. J. Lee, Appl. Phys. Lett. **81**, 3648 (2003).
[3] C. X. Xu and X. W. Sun, Appl. Phys. Lett. **83**, 3806 (2003).
[4] C. X. Xu, X. W. Sun, and B. J. Chen, Appl. Phys. Lett. **84**, 1540 (2004).
[5] H. Kind, H. Yan, B. Messer, M. Law, and P. Yang, Adv. Mater. (Weinheim, Ger.) **14**, 153 (2002).
[6] M. S. Arnold, P. Avouris, Z. W. Pan, and Z. L. Wang, J. Phys. Chem. B **107**, 659 (2003).
[7] X. Y. Kong, and Z. L. Wang, Nano Lett. **3**, 1625 (2004).
[8] G. A. Prinz, Science **282**, 1660 (1998).
[9] W. Prellier, A. Fouchet, and B. Mercey, J. Phys.: Condens. Matter **15**, R1583 (2003).
[10] A. F. Jalbout, H. Chen, and S. L. Whitternburg, Appl. Phys. Lett. **81**, 2217 (2002).
[11] C. Ronning, P. X. Gao, Y. Ding, and Z. L. Wang, Appl. Phys. Lett. **84**, 783 (2004).
[12] K. Ip, R. M. Frazier, Y. W. Heo, D. P. Norton, C. R. Abenathy, S. J. Pearton, J. Kelly, R. Rairigh, A. F. Hebard, J. M. Zavada, and R. G. Wilson, J. Vac. Sci. Technol. B **21**, 1476 (2003).